Experimental and numerical study of butt welded joints made of high strength steel

Yan, Rui; El Bamby, Hagar; Veljkovic, Milan

DOI
10.1201/9781003348443-190

Publication date
2023

Document Version
Final published version

Published in
Current Perspectives and New Directions in Mechanics, Modelling and Design of Structural Systems - Proceedings of the 8th International Conference on Structural Engineering, Mechanics and Computation, 2022

Citation (APA)
Yan, R., El Bamby, H., & Veljkovic, M. (2023). Experimental and numerical study of butt welded joints made of high strength steel. In A. Zingoni (Ed.), *Current Perspectives and New Directions in Mechanics, Modelling and Design of Structural Systems - Proceedings of the 8th International Conference on Structural Engineering, Mechanics and Computation, 2022* (pp. 1166-1171). CRC Press / Balkema - Taylor & Francis Group. https://doi.org/10.1201/9781003348443-190

Experimental and numerical study of butt welded joints made of high strength steel

Rui Yan
Hagar El Bamby
Milan Veljkovic
Faculty of Civil Engineering and Geosciences, Delft University of Technology, Delft, The Netherlands

ABSTRACT: Welded joints are wildly used in the construction sector for fabrication of steel and aluminium structures. A welded joint is traditionally divided into three regions: the base material (BM), the heat-affected zone (HAZ), and the weld material (WM). The mechanical behaviour of each region varies depending on properties of BM, FM and welding parameters. In general, HAZ has a lower material strength compared to BM and WM. The material strength difference is even more significant if BM is made of high strength steel (HSS) and welded by using undermatching electrodes. Therefore, it is essential to obtain the constitutive model of HAZ to accurately predict the behaviour (strength, stiffness, and ductility) of the HSS welded joint. In this paper, milled coupon specimens with a transverse butt weld in the middle are used for obtaining the original stress-strain relationship of HAZ and WM based on digital image correlation (DIC) measurements. The original and the modified HAZ constitutive model are validated against the milled and unmilled coupon specimens by finite element analysis (FEA). Comparing the FEA and experimental results, it can be concluded that the modified HAZ constitutive model is successfully validated. Finally, the tensile behaviour of the butt-welded square hollow section is investigated through FEA. It is found that the peak deformation would be significantly overestimated if the modified HAZ constitutive model is not used.

1 INTRODUCTION

Welded joints are wildly used in the construction sector. A welded joint consists of three major regions, which are the base material (BM), the heat-affected zone (HAZ), and the weld material (WM). Compared to BM and WM, HAZ has a lower material strength. Therefore, accurately modelling HAZ behaviour plays a key role in the advanced simulation of welded joints.

Lockwood and Reynolds [1] investigated the tensile behaviour of friction stir welded aluminium joints. The milled thin (2.5 mm) and unmilled thick (8 mm) coupon specimens were tested in tension. It was found that the yield strength of the weak (HAZ) and the strong (BM and WM) region in the thin specimen was lower and higher, respectively than in the thick specimen. The yield strength difference is due to the transverse constraint in the thickness direction. The transverse constraint exists not only at the yield stage but also the ultimate stage. Hochhauser et al. [2] found that the tensile strength of the thick specimen is higher than the thin specimen at the onset of necking. Therefore, BM and WM may impose a transverse constraint in the thickness direction on HAZ during the entire tensile loading, given that HAZ has a lower yield and tensile strength than BM and WM. Similarly, the transverse constraint may also exist in the width direction of the milled thin specimen. Yan et al. [3] identified the transverse constraint at the boundary of two regions, such as BM and HAZ, in the milled thin specimen using digital image correlation (DIC). The longitudinal true strain in the loading direction and the transverse true strain perpendicular to the loading direction are extracted from measuring points along the loading direction. Under the uniaxial tensile stress state, the slope of the transverse strain-longitudinal strain relationship at the plastic stage should be -0.5, according to the volume preservation assumption. However, the slope is different from -0.5 under the biaxial stress around the regions' boundary. The slope variation along the loading direction demonstrates the existence of the transverse constraint, and the regions' boundary is identified accordingly.

Zhang et al. [4] investigated the tensile behaviour of the girth weld of the high-strength steel pipeline. The stress-strain relationship of HAZ was modified based on a trial-and-error process in order to eliminate the effect of the transverse constraint. The Ramberg-Osgood model was used to fit the true stress-strain curves. Yan et al. [5] proposed a method to modify the HAZ stress-strain relationship measured by DIC. A linear modification factor was used to modify the true stress at the plastic stage until the necking point. The modified HAZ stress-strain relationship was validated against the tensile coupon test by finite element analysis (FEA).

In this paper, the HAZ stress-strain relationship is calibrated using FEA for two HSS, S500 and S700, based on the tensile tests on the milled coupon specimen with a transverse butt weld in the middle. The modified stress-strain relationship is further verified by the tensile test of the unmilled welded coupon specimen. Finally, the one-quarter square hollow section (SHS) FE model is used to study the tensile behaviour of the welded SHS using the investigated material.

2 EXPERIMENTS

2.1 *Materials*

The Cold-formed SHSs made of HSS, S500 and S700, were used as BM in this study. The dimension of S500 and S700 SHS was 160×160×10 and 120×120×8, respectively.

Edges of two hollow section profiles with 200 mm length were prepared with a V groove bevel before welding. The profiles were butt welded using the metal active gas (MAG) welding process and preheated by an interpass temperature ranging from 20°C to 200°C to avoid hydrogen cracking. The heat input was in the range of 1 to 1.4 kJ/mm. The filler metal (electrode) Union Nimocr is used for both steel grades. The mechanical property of BM, obtained from the standard tensile coupon test, and the material property of the filler material, provided by the fabricator, are shown in Table 1. Comparing the strength of BM and the electrode, overmatching and undermatching electrodes were used to weld S500 and S700 SHS profiles, respectively.

Table 1 Mechanical property of the base material and the filler metal

Material	Yield strength [MPa]	Tensile strength [MPa]	A [%]
S500	593	630	21
S700	789	861	14
Union Nimocr	720	780	17

where A is the percentage elongation after the fracture based on the 5.65 coefficient of proportionality, according to [6].

2.2 *Experimental setup*

The standard coupon specimen used to obtain the base material property was fabricated from the welded tube, as shown in Figure 1. Two welded coupon specimens were fabricated for each steel grade. One welded coupon specimen was milled to a central thickness zone of 3 mm to have a perpendicular HAZ boundary through the thickness before the tensile test. Another welded coupon specimen was directly tested with the complete weld in the middle. In addition, a small sample, including the weld in the middle, was cut out and prepared for the metallurgical investigation.

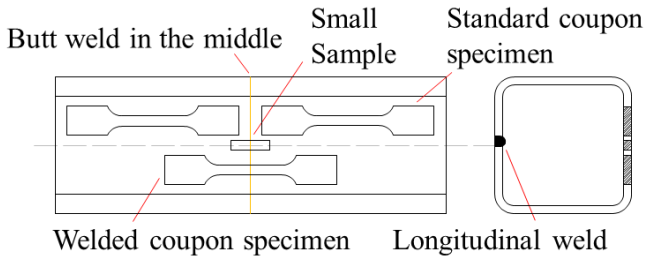

Figure 1 Specimen cutting scheme

The standard coupon test was conducted in an Instron testing machine with a 100 kN capacity. The loading rate was 0.01 mm/s with displacement control. 3D DIC was employed to measure the deformation during the test. The imaging resolution on the specimen, the subset size, and the step size was 67 microns/pixel, 9-pixel, and 5-pixel, respectively.

The small sample was prepared for the microstructure observation and the low-force Vickers hardness test (HV 0.5), based on a series of polishing and etching procedures.

3 FINITE ELEMENT ANALYSIS (FEA)

3.1 *Uniaxial stress-strain relationship*

The engineering stress-strain relationship of BM is obtained from the tensile test of the standard coupon test based on a 50 mm gauge length. A linear combination of the power law [7] and the linear law [8] is used to generate the BM undamaged true stress-true strain relationship, which is validated against the standard coupon test following the procedures proposed in [9]. The linear combination, the power law,

and the linear law are presented in Equation 1, Equation 2, and Equation 3, respectively.

$$\sigma_t[\varepsilon_t] = W\sigma_P[\varepsilon_t] + (1-W)\sigma_L[\varepsilon_t] \quad \text{Equation 1}$$

$$\sigma_P[\varepsilon_t] = A(\varepsilon_t + \varepsilon_0)^n \quad \text{Equation 2}$$

$$\sigma_L[\varepsilon_t] = a\varepsilon_t + b \quad \text{Equation 3}$$

where W is the weighting factor; A, ε_0, and n are the power law parameters; σ_P is the true stress predicted by the power law; a and b are the linear law parameters; σ_L is the true stress predicted by the linear law; σ_t and ε_t are the true stress and the true strain, respectively.

The stress-strain relationship of HAZ and WM is measured from the milled welded coupon specimen. Three contour plots of the true strain in the loading direction measured by DIC are shown in Figure 2. The only difference among the plots is the maximum value used in the legend. Obviously, the width of the "red stripe" reduces with the increase of the maximum value in the legend. It is not clear from which specific region the "pure" HAZ deformation should be measured. The slope of the longitudinal true strain-transverse true strain relationship, measured from single points, is used to identify HAZ boundaries, as proposed in [3]. The HAZ engineering stress-strain relationship is measured in the range of the identified boundaries.

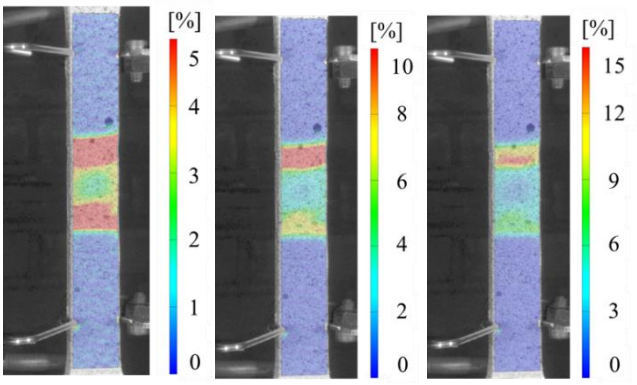

Figure 2 Strain distribution of S700 milled welded coupon specimen measured by DIC

BM and WM imposed a transverse constraint on HAZ during the tensile test of the milled coupon specimen at the plastic stage, indicating that HAZ was under a biaxial tensile stress state instead of a uniaxial tensile stress state. Consequently, the measured stress-strain relationship (the blue dash line in Figure 3) has a higher strength than under the uniaxial stress state (the red dash line in Figure 3) at the same strain level. Therefore, the method proposed by Yan et al. [5] is adapted to modify the measured stress-strain relationship. A linear modification factor is used to reduce the true stress of HAZ between yielding and necking, as shown in Figure 3.

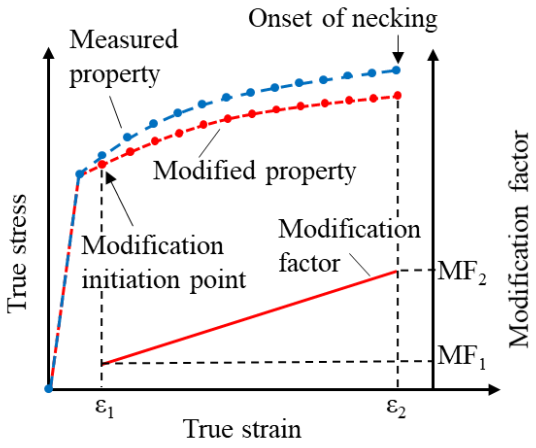

Figure 3 Schematic diagram of the linear stress modification factor

The stress-strain relationship of WM is measured from the centre 5 mm of WM. Lockwood and Reynolds [1] found that the yield strength of WM measured from the thick (without milling) and the thin (with milling) specimen was very close, indicating that the transverse constraint at the centre of WM is very limited. Therefore, it is assumed that the effect of the transverse constraint on the longitudinal deformation does not exist in the measuring range.

3.2 *Finite Element (FE) model*

The ABAQUS:2019 software package [10] is used to conduct FEA. The FE models for the milled and unmilled welded coupon specimens are made based on the measured dimensions, as shown in Figure 4 a) and b), respectively. The HAZ width in the milled specimen is in accordance with the identified width as introduced in Section 3.1. Regarding the HAZ geometry in the unmilled specimen, the result of the metallurgical investigation presented in Section 4.1 is used to confirm the boundaries of HAZ. In addition, using the cross-sectional geometry of the unmilled specimen, a FE model of a quarter welded SHS is created for S700 material, as shown in Figure 4 c). The dimension of SHS is the same as the S700 SHS used for fabricating the coupon specimen.

In the FE model of the milled and unmilled coupon specimen, a 0.5 mm fine mesh is applied within the 50 mm gauge length, while a coarse mesh is used for the remaining part. The FE model of the welded SHS only has the 0.5 mm fine mesh in the central weld region covering HAZ, WM, and 5 mm BM region close to HAZ boundary on both sides. Reference points (RP1 and RP2) are created in the centre of two end surfaces. Each reference point controls all translations and rotations of the corresponding end surface through the multi-point beam constraint (MPC beam). The load is applied by a positive displacement at RP2 in the Y direction. The remaining degrees of freedom at reference points are fixed. In addition, symmetric

boundary conditions are applied on surface A and surface B of welded SHS in order to model the tensile behaviour of the complete cross-section, as shown in Figure 4 c). The quasi-static analysis is conducted using the explicit solver with a 100 s period and a 0.0001 s target time increment. The eight-node hexahedral solid element with reduced integration (C3D8R) is used throughout the whole model except for a small transition zone (enlarging the element size in BM) where C3D10 is used.

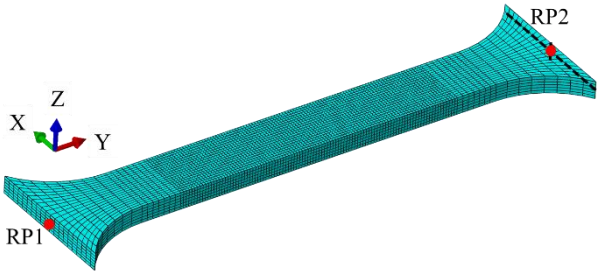

a) Milled welded coupon specimen

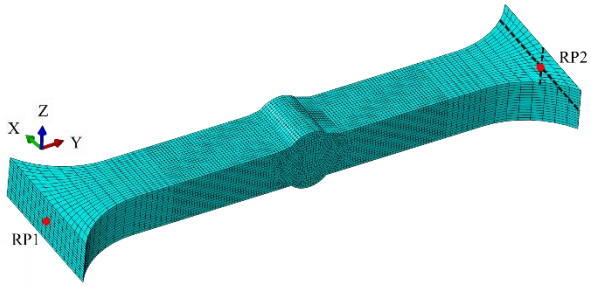

b) Unmilled welded coupon specimen

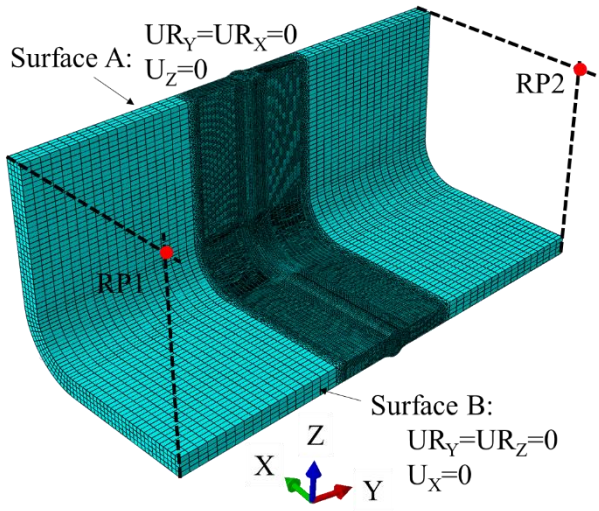

c) A quarter of welded SHS

Figure 4 Three FE models

4 RESULTS

4.1 *HV 0.5 Hardness and microstructure results*

The microstructure of the weld zone for each steel grade is shown in Figure 5. The red dash line represents the HAZ boundary determined based on the observed microstructure. In addition, the contour plot of HV 0.5 hardness result is also presented in Figure 5. Since HAZ is weaker than BM and WM in terms of the material strength, a lower hardness is expected in HAZ. It can be seen that the low hardness region aligns with the HAZ region identified by the microstructure. Therefore, the dimension of WM and HAZ determined by the microstructure is used in the FE model of the unmilled coupon specimen and the quarter of welded SHS joint, as introduced in Section 3.2.

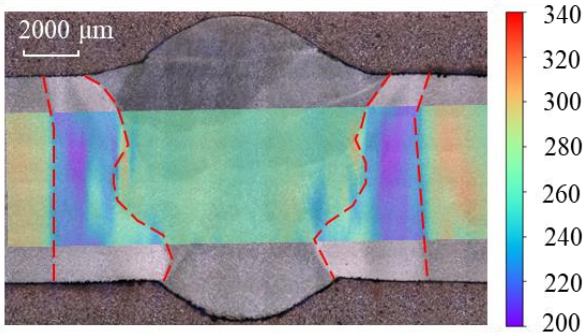

a) S700 weld zone

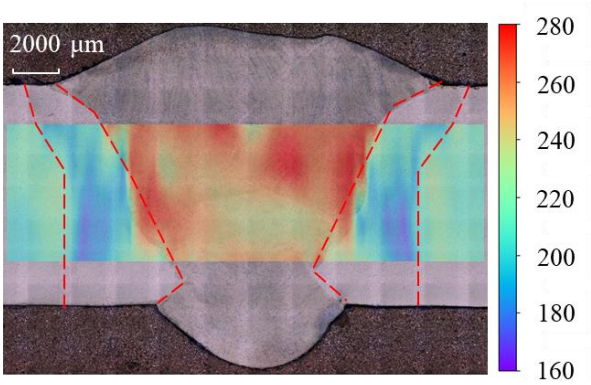

b) S500 weld zone

Figure 5 Hardness and microstructure results

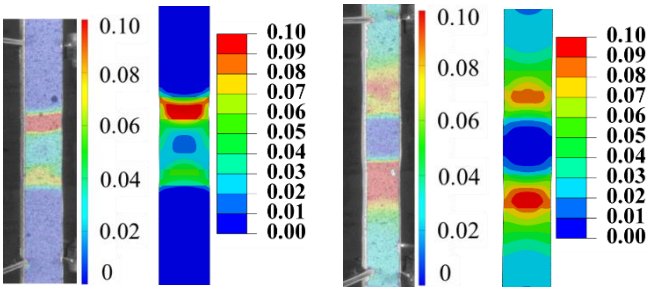

a) S700 specimen b) S500 specimen

Figure 6 True strain contour plot in the milled welded coupon specimen

4.2 *Tensile test results*

Figure 6 shows the contour plot of the true strain in the loading direction of the milled welded coupon

specimen at the ultimate load. Two high-strain regions, corresponding to two HAZs, exist on the specimen. The fracture also occurs in HAZ. However, regarding the unmilled welded coupon specimen in Figure 7, the high strain concentrates in HAZ for S700 while in BM for S500 at the ultimate load. The final failure appears in HAZ and BM for S700 and S500 specimens, respectively.

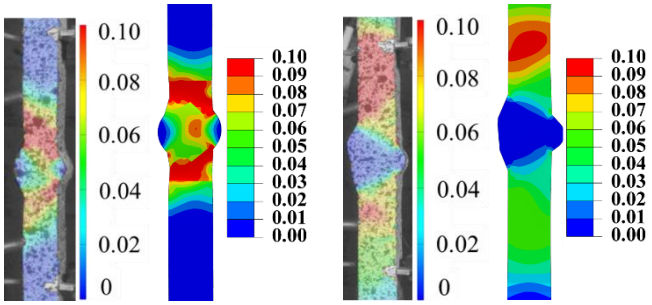

a) S700 specimen b) S500 specimen

Figure 7 True strain contour plot in the unmilled welded coupon specimen

4.3 *FE results*

Two HAZ constitutive models, the original model measured from DIC (corresponding to FEA-ori) and the modified model based on the linear modification factor (corresponding to FEA-mod), are used in FEA. Following the calibration procedures proposed in [5], the measured true stress of HAZ after the onset of yielding is reduced by 4% and 5% for S700 and S500, respectively. The true stress at necking is reduced by 8% and 0% for S700 and S500, respectively. The reduction between the yielding and the necking is linearly interpolated according to the true strain.

Figure 8 shows the load-deformation relationship of the milled welded specimen, the unmilled welded specimen, and the welded SHS in a), b), and c), respectively. The full experimental curve is presented while the FE curves are plotted until the ultimate load. The ultimate load point is marked by a solid "star" with the same colour as the corresponding curve.

The experimental and FE results of the milled welded coupon specimen are compared in Figure 8 a). The ultimate resistance and the peak deformation of the S500 specimen are well predicted using both the measured original and the modified HAZ stress-strain relationship since the HAZ stress is not substantially reduced at the onset of the necking. For the S700 specimen, using the original HAZ constitutive model, the ultimate resistance is slightly overestimated by 5%, while the peak deformation has a 30% overestimation. The ultimate resistance and the peak deformation are well predicted with less than 1% deviation using the modified HAZ constitutive model. The contour plot of the strain in the FE model using the modified HAZ constitutive model is compared to the experimental result in Figure 6. It can be seen that the FE results match the experimental results well.

Figure 8 b) shows the load-deformation relationship of the unmilled welded specimen. Similar to the milled specimen, the FE model using the original and modified HAZ property does not show a significant difference in the predicted resistance and deformation at the ultimate stage for the S500 specimen. However, for the S700 specimen, the FE model overestimates the ultimate resistance and peak deformation by 5% and 14%, respectively, using the original HAZ property. The FE result deviates less than 1% from the experimental result using the modified HAZ property. The strain contour plot of the FE model using the modified HAZ property shows good agreement with the experiment, as shown in Figure 7. The position of the high-strain region (in HAZ for S700 specimen and in BM for S500 specimen) is well predicted.

The welded SHS joint was not tested in the experiment. A FE study is carried out to investigate the overestimation of the peak deformation using the original and modified HAZ property. In addition, a FE model using the BM property for all three regions (BM, HAZ, and WM), shown as FEA-BM, is made for comparison. Since BM governs the resistance and the failure of the S500 unmilled welded joint, the different HAZ stress-strain relationships would not significantly affect the behaviour of the welded SHS. Therefore, only the S700 material is investigated in this study. Figure 8 c) compares the load-deformation relationship obtained from FE models based on a 200 mm gauge length. Compared to the model using the modified HAZ property, the model using the original HAZ property and BM property have a 2% and 4% higher resistance, respectively, while a 49% and 34% higher peak deformation, respectively.

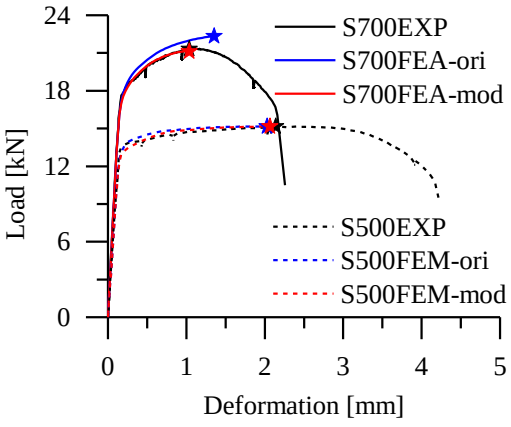

a) Milled welded coupon specimen

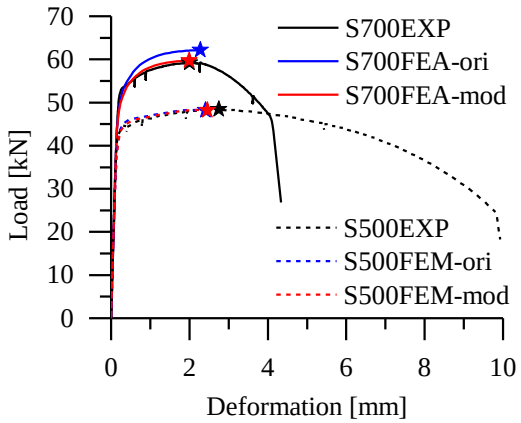

b) Unmilled welded coupon specimen

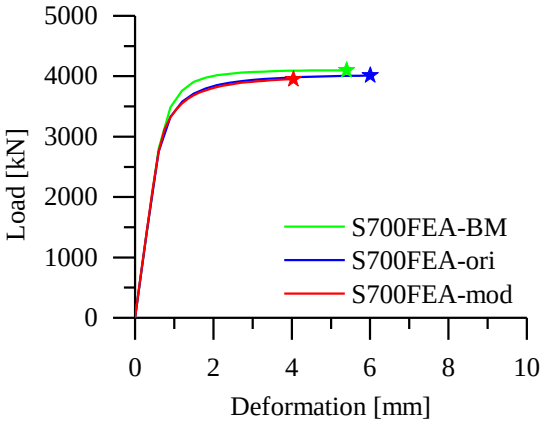

c) Welded SHS

Figure 8 Load-deformation relationship

5 CONCLUSIONS

This research is a part of an ongoing project: the tensile behaviour of welded RHS X-joints. S500 and S700 weld joints under different scales are investigated in this paper. Following conclusions are drawn:

1. The HAZ true stress for the S700 specimen (undermatching weld) should be reduced by 4% and 8% at the yielding and necking stage. The ultimate resistance of the milled and unmilled welded coupon specimen is overestimated by less than 5% by FEA using the original HAZ property. However, the predicted peak deformation is 30% and 14% larger than the experimental result for the milled and unmilled specimens, respectively. Using the modified HAZ material property, the predicted ultimate resistance and peak deformation deviate less than 1% from the experimental results.

2. For S500 overmatching welded specimen, a 5% and 0% reduction are made at the yielding and necking stage. Since no reduction is necessary for S500 HAZ at the onset of the necking, the peak deformation and the ultimate resistance predicted by FEA using the original and the modified HAZ stress-strain relationship show a minor difference.

3. Regarding the butt welded S700 SHS joint, the ultimate resistance predicted by FEA using the original HAZ material, the modified HAZ material, and the BM property, has a maximum of 4% scattering. However, compared to the FE model using the modified HAZ property, the model using the original HAZ property and BM property have a 49% and 34% larger peak deformation, respectively.

REFERENCE

[1] W.D. Lockwood, A.P. Reynolds, Simulation of the global response of a friction stir weld using local constitutive behavior, Materials Science and Engineering A. 339 (2003) 35–42. doi.org/10.1016/S0921-5093(02)00116-8.

[2] F. Hochhauser, W. Ernst, R. Rauch, R. Vallant, Influence of the soft zone on the strength of welded modern HSLA steels, Welding in the World. 56 (2012). doi.org/10.1007/BF03321352.

[3] R. Yan, H. El Bamby, M. Veljkovic, H. Xin, F. Yang, A method for identifying the boundary of regions in welded coupon specimens using digital image correlation, Materials & Design. 210 (2021) 110073. doi.org/10.1016/j.matdes.2021.110073.

[4] Y. Zhang, J. Shuai, W. Ren, Z. Lv, Investigation of the tensile strain response of the girth weld of high-strength steel pipeline, Journal of Constructional Steel Research. 188 (2022) 107047. doi.org/10.1016/j.jcsr.2021.107047.

[5] R. Yan, H. Xin, F. Yang, H. El Bamby, M. Veljkovic, K. Mela, A method for determining the constitutive model of the heat-affected zone using digital image correlation (submitted), Construction and Building Materials.

[6] Metallic materials - Tensile testing - Part 1: Method of test at room temperature (ISO 6892-1:2019), 1 (2019).

[7] H.W. Swift, Plastic instability under plane stress, Journal of the Mechanics and Physics of Solids. 1 (1952) 1–18. doi.org/10.1016/0022-5096(52)90002-1.

[8] Y. Ling, Uniaxial True Stress-Strain after Necking, AMP Journal of Technology. 5 (2004) 37–48.

[9] R. Yan, H. Xin, M. Veljkovic, Ductile fracture simulation of cold-formed high strength steel using GTN damage model, Journal of Constructional Steel Research. 184 (2021) 106832. doi.org/10.1016/j.jcsr.2021.106832.

[10] ABAQUS, Abaqus Analysis User's Manual, 2019 version, (2019).